Inorg. Chem. **2008**, *47*, 10758−10764

CuO Particles from Ionic Liquid/Water Mixtures: Evidence for Growth via $Cu(OH)_2$ Nanorod Assembly and Fusion

Andreas Taubert,*[,†,‡] Annett Uhlmann,[†] Annett Hedderich,[†] and Katrin Kirchhoff[§]

Institute of Chemistry, University of Potsdam, D-14476 Golm, Germany, Max-Planck-Institute of Colloids and Interfaces, D-14476 Golm, Germany, and Max-Planck-Institute for Polymer Research, D-15528 Mainz, Germany

Received July 17, 2008

Tetrabutylammonium hydroxide/water mixtures are efficient reaction media for the fabrication of nanoscale metal oxides and hydroxides. Uniform CuO nanoplates, among others, can be grown on a large scale. This work shows that after 30 s at temperatures above 40 °C, CuO formation is already essentially complete. X-ray diffraction and transmission electron microscopy (TEM) show that the resulting plates form via a two-step process, where $Cu(OH)_2$ rods precipitate first. These rods aggregate and fuse into plates with a width/height ratio of about 1.9. High-resolution TEM and electron diffraction show that the plates are single crystals and exhibit only some defects, which most likely originate from the assembly and fusion of the primary rods.

Introduction

Metal oxides and hydroxides have found numerous applications in the catalysis, data storage, energy technology, and coatings fields, to name a few examples.[1,2] Over the last few decades, metal oxide nanoparticles have therefore been one of the key areas of inorganic materials research. Despite the extensive experience in inorganic nanoparticle synthesis, new synthetic protocols for advanced inorganic nanoparticles are still being developed.[3−7] Also, the understanding of the processes by which crystals grow has been deepened by recent research on nanoparticles.[8−13]

For example, Banfield and colleagues have put forward the concept of oriented attachment.[9] In this concept, larger crystalline entities form by the attachment and fusion of nanoparticles. During this process, the crystallographic correlation among the individual building blocks is maintained, and the resulting larger structure is a crystallographically highly correlated material.

Cölfen and colleagues have put forward the concept of mesocrystals.[10,11] Mesocrystals have a defined morphology and a single-crystal-like appearance. Unlike single crystals, mesocrystals form via the assembly of nanometer-sized (anisotropic) primary particles.[10−20] Mesocrystal formation and growth have been attributed to oriented aggregation of individual, small particles such that the resulting larger crystals have an overall single-crystal-like orientation.[13,14]

* To whom correspondence should be addressed. E-mail: ataubert@uni-potsdam.de. Phone: ++49 (0)331 977 5773. Address: Institute of Chemistry, University of Potsdam, Karl-Liebknecht-Strasse 24-25, Building 26, D-14476 Golm, Germany.
† University of Potsdam.
‡ Max-Planck-Institute of Colloids and Interfaces.
§ Max-Planck-Institute for Polymer Research.

(1) Jolivet, J. P. *Metal Oxide Chemistry and Synthesis: From Solution to Solid State*; John Wiley & Sons: New York, 2000.
(2) Cornell, R. M.; Schwertmann, U. *The Iron Oxides: Structure, Properties, Reactions, Occurrences and Uses*; Wiley-VCH: Weinheim, Germany, 2003.
(3) Ba, J. H.; Polleux, J.; Antonietti, M.; Niederberger, M. *Adv. Mater. (Weinheim, Ger.)* **2005**, *17*, 2509.
(4) Niederberger, M. *Acc. Chem. Res.* **2007**, *40*, 793.
(5) Niederberger, M.; Krumeich, F.; Hegetschweiler, K.; Nesper, R. *Chem. Mater.* **2002**, *14*, 78.
(6) Feldmann, C. *Adv. Mater. (Weinheim, Ger.)* **2001**, *13*, 1301.
(7) Feldmann, C.; Metzmacher, C. *J. Mater. Chem.* **2001**, *11*, 2603.
(8) Banfield, J. F.; Welch, S. A.; Zhang, H.; Thomsen Ebert, T.; Penn, R. L. *Science* **2000**, *289*, 751.
(9) Penn, R. L.; Banfield, J. F. *Science* **1998**, *281*, 969.
(10) Cölfen, H.; Antonietti, M. *Angew. Chem., Int. Ed.* **2005**, *44*, 5576.
(11) Wang, T.; Cölfen, H.; Antonietti, M. *J. Am. Chem. Soc.* **2005**, *127*, 3246.
(12) Wang, T.; Cölfen, H.; Antonietti, M. *Chem.—Eur. J.* **2006**, *12*, 5722.
(13) Niederberger, M.; Cölfen, H. *Phys. Chem. Chem. Phys.* **2006**, *8*, 3271.
(14) Cölfen, H.; Mann, S. *Angew. Chem., Int. Ed.* **2003**, *42*, 2350.
(15) Hsu, W. P.; Rennquist, L.; Matijevic, E. *Langmuir* **1988**, *4*, 31.
(16) Xu, A.-W.; Antonietti, M.; Cölfen, H.; Fang, Y.-P. *Adv. Funct. Mater.* **2006**, *16*, 903.
(17) Wohlrab, S.; Pinna, N.; Antonietti, M.; Cölfen, H. *Chem.—Eur. J.* **2005**, *11*, 2903.
(18) Chen, S.; Yu, S.; Wang, T.; Jiang, J.; Cölfen, H.; Hu, B.; Yu, B. *Adv. Mater. (Weinheim, Ger.)* **2005**, *17*, 1461.
(19) Ma, Y.; Cölfen, H.; Antonietti, M. *J. Phys. Chem. B* **2006**, *110*, 10822.
(20) Page, M. G.; Cölfen, H. *Cryst. Growth Des.* **2006**, *6*, 1915.

10.1021/ic801335k CCC: $40.75
Published on Web 10/21/2008

Alternatively, the formation and growth have been attributed to intrinsic electric fields, which control the orientation of the individual primary building blocks.[21,22]

Typically, aqueous and organic solvents have been used for inorganic nanoparticle synthesis.[4,23] More recently, ionic liquids (ILs) have also been used successfully for the synthesis of inorganic materials and surfaces.[24−29] In some cases, ILs lead to materials that are not accessible via other methods,[26,29−35] and in a few cases, ILs have been shown to be solvents for metal oxides.[36] For example, condensation reactions in ILs provide easy access to hollow TiO_2 spheres,[32] and ionothermal synthesis leads to well-defined metal phosphates.[29,33,37−40] ILs also enable the controlled, low-temperature synthesis of anatase and rutile,[34] ceria and silica with well-defined pores,[24,41,42] and different phases of alumina.[43] Therefore, ILs are an interesting alternative for the fabrication of inorganic nanostructures. As a result, inorganic synthesis in ILs, including mixtures of ILs with other solvents like water or toluene, has been studied intensely over the last few years.[24,25,28,29,37,44]

Originally, ILs were used as solvents and solvent/templates. We have recently put forward the concept of using ionic liquid crystal precursors (ILCPs)[45−48] for the synthesis of inorganic materials, and Zhu et al. have more recently reported on using the first ionic liquid precursor (ILP) for the synthesis of inorganic particles.[49] Other research groups have modified these approaches to fabricate inorganics with well-defined properties.[50−52]

Zhu et al. have shown that tetramethylammonium hydroxide is an ILP for the ionothermal synthesis of well-defined ZnO microparticles.[49] We have extended this approach and have shown that mixtures of water and the IL tetrabutylammonium hydroxide (TBAH), which is the butyl analog of the compound used by Zhu et al., are effective reaction media for the synthesis of metal oxide particles with different architectures. Among others, TBAH is an ILP for the controlled fabrication of unique, hollow zinc oxide mesocrystals and for ZnO−carbohydrate hybrid materials.[53,54]

This work shows that after 30 s at temperatures above 40 °C, CuO formation in TBAH is already essentially complete. X-ray diffraction (XRD) and transmission electron microscopy (TEM) show that the resulting plates form via a two-step process, where $Cu(OH)_2$ rods precipitate first. These rods aggregate and fuse into plates with a width/height ratio of about 1.9. High-resolution TEM and electron diffraction show that the plates are single crystals and exhibit only some defects, which most likely originate from the assembly and fusion of the primary rods.

Experimental Section

Mineralization. In a typical synthesis, 0.083 g of copper acetate (98%, Aldrich) was dissolved in 2 mL of water. The mixture was briefly sonicated at room temperature, yielding a concentration of 0.2280 mmol/mL. Ten grams of tetrabutylammonium hydroxide [TBAH, $N(C_4H_9)_4OH \cdot 30H_2O$, Fluka, mp 26−28 °C] was heated in a 25 mL round-bottomed flask with a reflux condenser to the desired reaction temperature. The aqueous copper acetate solution was injected rapidly into the liquid TBAH. After a few seconds, the solution turned brown and remained so until the end of the reaction. The reaction was terminated by rapidly cooling the reaction flask in an ice bath, followed by centrifugation at 4000 rpm for 10 min. The samples were washed twice with water, washed once with ethanol, and dried at 90 °C.

Characterization. XRD was done on a Nonius PDS 120 with Cu Kα radiation and a position sensitive detector and on a Nonius D8 with Cu Kα radiation. For electron microscopy, samples were dispersed in ethanol, sonicated, and deposited on carbon-coated copper grids. TEM was done on a Zeiss 912 Omega operated at 120 kV. TEM tilt experiments and high-resolution TEM (HRTEM) were done on an FEI Tecnai F20 with a single-tilt holder operated at 200 kV. Image analysis and determination of particle volumes and particle numbers were done using OriginLab Origin 6.1 as described previously.[55] Simulation of electron diffraction patterns was done with EMS Online[56] using the experimental TEM

(21) Busch, S.; Dolhaine, H.; DuChesne, A.; Heinz, S.; Hochrein, O.; Laeri, F.; Podebrad, O.; Vietze, U.; Weiland, T.; Kniep, R. *Eur. J. Inorg. Chem.* **1999**, (10), 1643.
(22) Busch, S.; Schwarz, U.; Kniep, R. *Adv. Funct. Mater.* **2003**, *13*, 189.
(23) Schweizer, S.; Taubert, A. *Macromol. Biosci.* **2007**, *7*, 1085.
(24) Antonietti, M.; Kuang, D.; Smarsly, B.; Zhou, Y. *Angew. Chem., Int. Ed.* **2004**, *43*, 4988.
(25) Taubert, A.; Li, Z. *Dalton Trans.* **2007**, (7), 723.
(26) Endres, F. *Proc.−Electrochem. Soc.* **2002**, *677*, 2002–2019.
(27) Endres, F.; Abedin, S. Z. E. *Phys. Chem. Chem. Phys.* **2006**, *8*, 2101.
(28) Reichert, W. M.; Holbrey, J. D.; Vigour, K. B.; Morgan, T. D.; Broker, G. A.; Rogers, R. D. *Chem. Commun. (Cambridge, U.K.)* **2006**, 4767.
(29) Parnham, E. R.; Morris, R. E. *Acc. Chem. Res.* **2007**, *40*, 1005.
(30) Moustafa, E. M.; Zein El Abedin, S.; Shkurankov, A.; Zschippang, E.; Saad, A. Y.; Bund, A.; Endres, F. *J. Phys. Chem. B* **2007**, *111*, 4693.
(31) Zein El Abedin, S.; Endres, F. *ChemPhysChem* **2006**, *7*, 58.
(32) Nakashima, T.; Kimizuka, N. *J. Am. Chem. Soc.* **2003**, *125*, 6386.
(33) Parnham, E. R.; Wheatley, P. S.; Morris, R. E. *Chem. Commun. (Cambridge, U.K.)* **2006**, 380.
(34) Kaper, H.; Endres, F.; Djerdj, I.; Antonietti, M.; Smarsly, B. M.; Maier, J.; Hu, Y.-S. *Small* **2007**, *3*, 1753.
(35) Nockemann, P.; Thijs, B.; Van Hecke, K.; Van Meervelt, L.; Binnemans, K. *Cryst. Growth Des.* **2008**, *8*, 1353.
(36) Nockemann, P.; Thijs, B.; Pittois, S.; Thoen, J.; Glorieux, C.; van Hecke, K.; van Meervelt, L.; Kirchner, B.; Binnemans, K. *J. Phys. Chem. B* **2006**, *110*, 20978.
(37) Cooper, E. R.; Andrews, C. D.; Wheatley, P. S.; Webb, P. B.; Wormald, P.; Morris, R. E. *Nature* **2004**, *430*, 1012.
(38) Parnham, E. R.; Morris, R. E. *J. Mater. Chem.* **2006**, *16*, 3682.
(39) Parnham, E. R.; Morris, R. E. *Chem. Mater.* **2006**, *18*, 4882.
(40) Parnham, E. R.; Morris, R. E. *J. Am. Chem. Soc.* **2006**, *128*, 2204.
(41) Brezesinski, T.; Erpen, C.; Iimura, K.; Smarsly, B. *Chem. Mater.* **2005**, *17*, 1683.
(42) Wang, T.; Kaper, H.; Antonietti, M.; Smarsly, B. *Langmuir* **2007**, *23*, 1489.
(43) Farag, H. K.; Endres, F. *J. Mater. Chem.* **2008**, *18*, 442.
(44) Morris, R. E. *Angew. Chem., Int. Ed.* **2008**, *47*, 443.
(45) Taubert, A. *Angew. Chem., Int. Ed.* **2004**, *43*, 5380.
(46) Taubert, A.; Arbell, I.; Mecke, A.; Graf, P. *Gold Bull. (London, U.K.)* **2006**, *39*, 205.
(47) Taubert, A.; Palivan, C.; Casse, O.; Gozzo, F.; Schmitt, B. *J. Phys. Chem. C* **2007**, *111*, 4077.
(48) Taubert, A.; Steiner, P.; Mantion, A. *J. Phys. Chem. B* **2005**, *109*, 15542.
(49) Zhu, H.; Huang, J.-F.; Pan, Z.; Dai, S. *Chem. Mater.* **2006**, *18*, 4473.
(50) Dobbs, W.; Suisse, J.-M.; Douce, L.; Welter, R. *Angew. Chem., Int. Ed.* **2006**, *45*, 4179.
(51) Lee, C. K.; Vasam, C. S.; Huang, T. W.; Wang, H. M. J.; Yang, R. Y.; Lee, C. S.; Lin, I. J. B. *Organometallics* **2006**, *25*, 3768.
(52) Kim, K.-S.; Choi, S.; Cha, J.-H.; Yeon, S.-H.; Lee, H. *J. Mater. Chem.* **2006**, *16*, 1315.
(53) Li, Z.; Gessner, A.; Richters, J. P.; Kalden, J.; Voss, T.; Kübel, C.; Taubert, A. *Adv. Mater. (Weinheim, Ger.)* **2008**, *20*, 1279.
(54) Mumalo-Djokic, D.; Stern, W. B.; Taubert, A. *Cryst. Growth Des.* **2008**, *8*, 330.
(55) Taubert, A.; Palms, D.; Glasser, G. *Langmuir* **2002**, *18*, 4488.
(56) Stadelmann, P. EMS Online. http://cecm.insa-lyon.fr/CIOL/1995−1998 (accessed June 13, 2008).

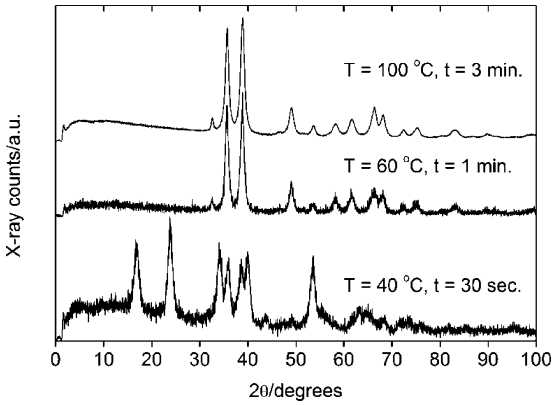

Figure 1. Representative XRD patterns of samples. The top two patterns can be assigned to tenorite (CuO, ICDD 00−045−0937). The lower pattern can be assigned to spertiniite [$Cu(OH)_2$, ICDD 00−35−0505].

parameters (200 kV, different camera lengths) as inputs. Atomic force microscopy (AFM) was done at ambient conditions on a Veeco NanoScope IIIa in tapping mode with silicon nitride tips (Nano World, $T = 4.6\ \mu m$, $L = 160\ \mu m$, force constant = 42 N/m, resonance frequency = 285 kHz). Samples were deposited onto mica, and particle heights were determined from the height images. Thermogravimetric analysis (TGA) and differential thermal analysis (DTA) measurements were done in a stationary air atmosphere (no purge) from 30 to 800 °C using a Linseis L81 thermal analyzer working in vertical mode. The heating rate was 5−10 °C/min, and Al_2O_3 was used as the reference material.

Results and Discussion

TGA shows that the samples contain less than 3% organic material, which decomposes upon heating (data not shown). Therefore, the majority of the material is inorganic precipitate.

Figure 1 shows powder XRD patterns of several samples isolated after various reaction times and from different reaction temperatures. The patterns of all samples obtained at 60, 80, and 100 °C can be assigned to single-phase CuO (tenorite, ICDD 00-045-0937). The samples synthesized at 40 °C are pure CuO after reaction times of 1 min or more. XRD of samples isolated after 30 s at 40 °C typically shows a pattern indicative of $Cu(OH)_2$ (spertiniite, ICDD 00-35-0505). CuO reflections are observed here occasionally. This indicates the formation of the CuO proceeds via a $Cu(OH)_2$ intermediate, which can be observed directly only at 40 °C and after 30 s of reaction time.

The efficiency of the $Cu(OH)_2$-to-CuO transformation is indicated further by the short induction times and the color of the reaction mixture. At 100 °C, the reaction mixture turns dark brown immediately after injection of the copper acetate solution. The brown color is indicative of the presence of CuO. At 80 °C, the induction period is about 3 s, at 60 °C about 10 s, and at 40 °C between 30 and 50 s. However, only at 40 °C is a blue precipitate, which is indicative of $Cu(OH)_2$, observed first after 30−50 s, before it turns brown after another few seconds.

Figure 2 shows TEM data of samples isolated from different reactions. At 40 °C and 30 s of reaction time, long bundles of rodlike crystals form. All other samples, with longer reaction times and higher temperatures, have platelike morphologies. Higher-magnification images of the latter

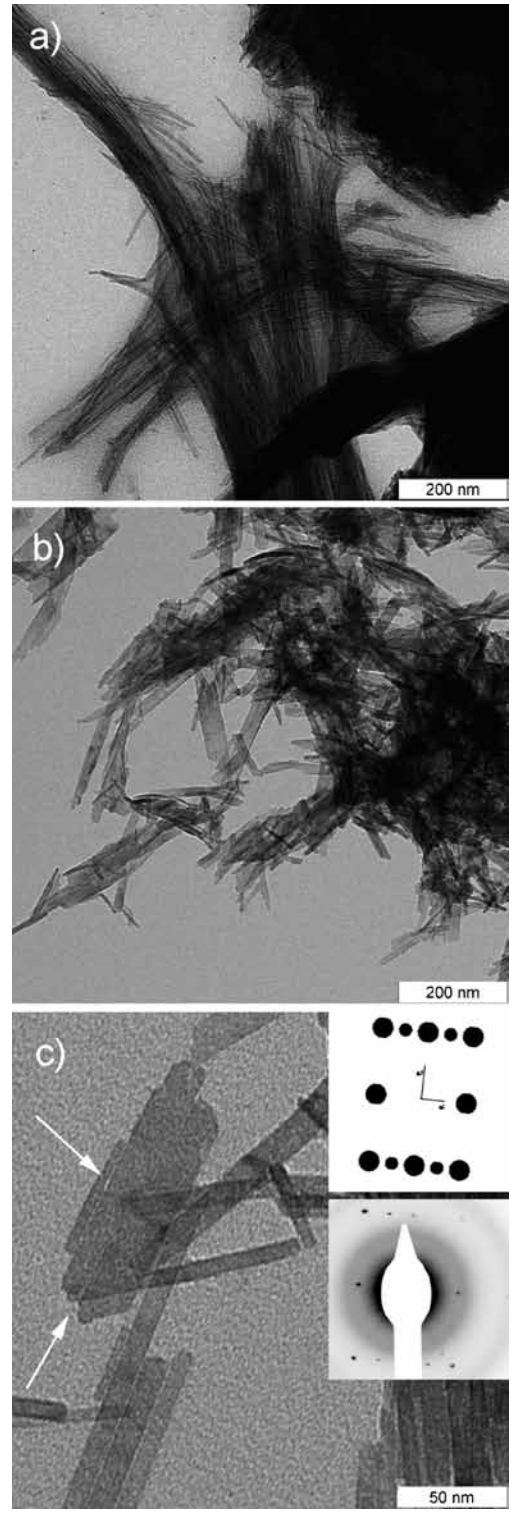

Figure 2. TEM images of (a) a sample isolated after 30 s from a solution at 40 °C and (b) a sample obtained after 5 min at 100 °C and (c) a high-magnification image of a particle obtained after 5 min at 100 °C. Crystals in panel b are representative of all samples obtained at 40 °C with more than 30 s of reaction time and samples obtained at higher temperatures. Arrows in panel c point to gaps or holes between the rodlike, primary particles. Insets in panel c show simulated (top) and experimental selected area electron diffraction (SAED) (bottom) patterns of a CuO particle. SAED patterns were obtained from several isolated particles and not from the region shown.

samples show that the plates seem to be composed of multiple rods, which are aligned in parallel. This suggests

these particles form by aggregation of primary rods, similar to those shown in Figure 2a. In some cases, gaps or holes between the rods can be observed. The gaps are interpreted as regions where the initial rods did not fill all available space either because of a slight misalignment or because one of the primary rods had a dent or step in the side face.

Besides the presence of the rodlike features, the tip shapes of the crystals also support the model of aggregating rods. Many tips do not have shapes that can be assigned to one single crystal; rather, the tips appear to be the ends of the respective original rods that have grown together to form the final crystal. As a result, TEM and XRD suggest that $Cu(OH)_2$ precipitates initially, although this first stage can be observed only at 40 °C. The $Cu(OH)_2$ rods then quickly fuse to form platy structures, via a side-by-side attachment of the primary rods.

Presently, it is difficult to determine whether the plates form only by rod-to-rod attachment or if additional growth processes take place. This is mostly because the length and width distributions of both rods and plates are broad, and a statistical analysis is difficult. However, TEM suggests most of the plate formation is due to aggregation of the rods because no major growth in either the length of the rods or the length of the plates is observed.

SAED shows that the particles are single crystals because sharp spots are observed. The SAED patterns can be assigned to the [100] zone axis, which show the long axis of the CuO particles is the *c*-axis. All reflections predicted by the simulation were observed, although some of them were weak.

Figure 3 shows the corresponding HRTEM data of a sample obtained after 5 min from a 100 °C solution. HRTEM shows that the individual rods are single-crystalline particles because the lattice fringes extend throughout the whole particle. The lattice spacings of $d = 2.80$ and 2.30 Å can be assigned to the $\bar{1}10$ and 200 planes (ICDD 00-045-0937), indicating the long crystal axis is the *c*-axis.

Therefore, HRTEM confirms SAED because it also shows that the *c*-axis is the long particle axis and the individual particles are single crystals. HRTEM also shows that, while the overall correlation of the individual, primary rods is high, there are defects such as edge dislocations. Furthermore, there are regions where no fringes are observed. These regions could be defects, but this issue could not be resolved. Overall, HRTEM is consistent with many other publications showing solution-grown particles can have a high order but are usually not free of defects.

Finally, HRTEM shows that the crystallographic correlation between the aggregated rods is high; in many cases, the lattice fringes of neighboring rods are in perfect register, suggesting that during aggregation there is a crystallographic correlation among the individual rods. This supports the TEM data that suggest the platelike particles shown in Figure 2 form via aggregation of individual rods. An oriented aggregation process also would be consistent with earlier data on TiO_2.[9] FFTs support these findings with clear spot patterns where almost identical orientations are found.

An aggregation-based growth is supported further by the crystal structures of $Cu(OH)_2$ and CuO. The long axis of

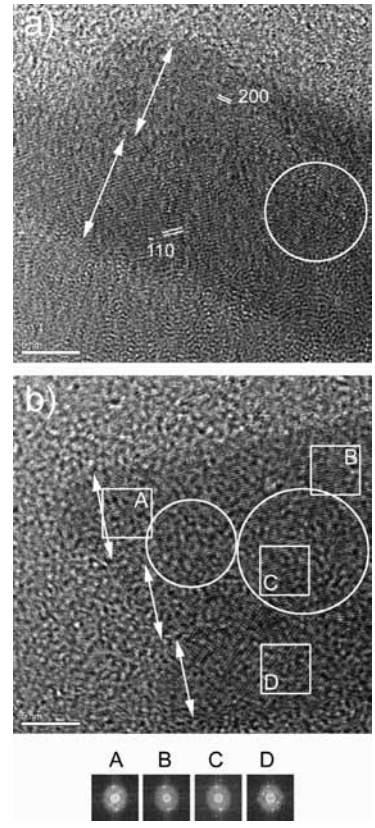

Figure 3. HRTEM images of CuO nanoparticles obtained after 5 min at 100 °C: (a) two aggregated rods, (b) three aggregated rods. Double-headed arrows indicate the widths of individual nanorods. Circles highlight areas where the lattice fringes continue uninterrupted across neighboring rods. The large circle in panel b highlights a region where the lattice fringes extend from the first rod to the third rod without interruption. Squares highlight regions where the fast Fourier transforms (FFTs) shown below in A−D were taken.

$Cu(OH)_2$ is the crystallographic *b*-axis, but in CuO the long axis is the *c*-axis.[57,58] In both crystal structures, Cu and O or OH, respectively, are arranged in alternating layers, which are perpendicular to the long *b*- or *c*-axis. As a result, $Cu(OH)_2$ rods can assemble first into aggregates of parallel rods. In these aggregated rods, copper and hydroxide form alternating layers perpendicular to the long particle axis. The transformation to CuO then occurs via condensation. However, during the dehydration process, the Cu and remaining O atoms do stay in register. Therefore, the resulting CuO particles have the copper and oxygen layers still perpendicular to the long crystal axis. As a final consequence, the order of the CuO particles is not disrupted by the fusion and condensation of the $Cu(OH)_2$ rods because the Cu and O layers continue across the boundaries of the individual rods, and the resulting particles are single crystals. Scheme 1 illustrates the model.

In order to determine if the platelike crystals are real plates, TEM tilt experiments were performed. Figure 4 clearly shows the assignment of a platelike morphology is too simple because in tilt experiments ranging from +50 to −50°,

(57) Wyckoff, R. W. G. *Crystal Structures*, 2nd ed.; Interscience Publishers: New York, 1963; Vol. *1*, p 85.
(58) Oswald, H. R.; Reller, A.; Schmalle, H. W.; Dubler, E. *Acta Crystallogr., Sect. C* **1990**, *46*, 2279.
(59) Barthelmy, D. Mineralogy Database. http://webmineral.com/.

Scheme 1. Suggested Growth Model for CuO Nanoplates by Aggregation of $Cu(OH)_2$ Nanorods and Subsequent Fusion by Dehydration[a]

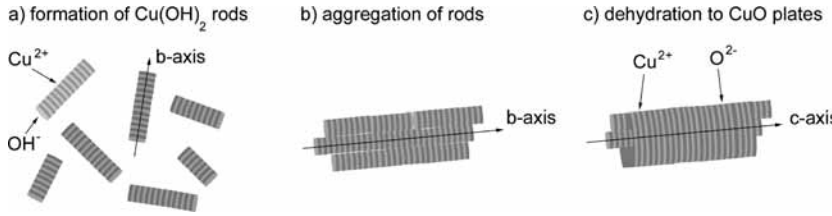

[a] During the transformation from $Cu(OH)_2$ to CuO, the relative orientation of the Cu, OH, and O layers is conserved. Dark gray indicates Cu layers, and light gray indicates OH or O layers. To study the crystallography of the process in more detail, the authors refer to ref 59 where rotation and visualization operations can be conducted free of charge, and the two crystal structures can be compared.

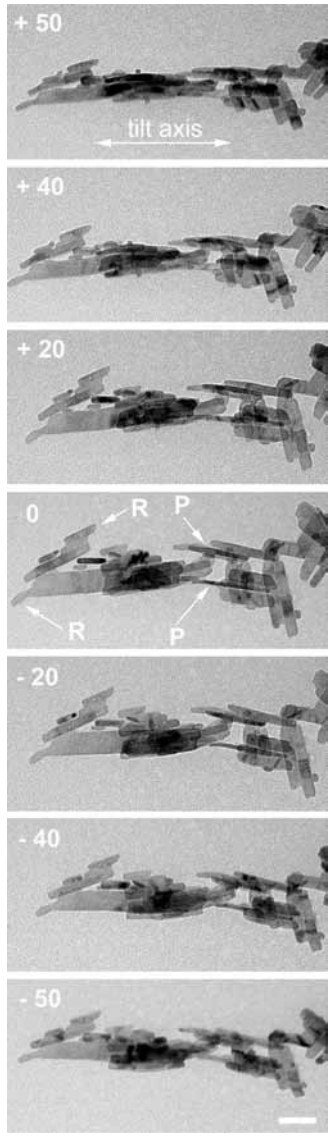

Figure 4. TEM tilt series of a set of CuO particles. The tilt series shows evidence for both plates and rods, although differentiation between the two types is not always straightforward. R: rods (no change in the shape during tilting). P: plates (transition between narrow and wide projection in the TEM image). Scale bar is 50 nm.

thickness variations could not always be observed. Rather, the width of the particles seems to be on the same order of magnitude as the thickness.

Because TEM images are a two-dimensional (2D) representation of a three-dimensional (3D) structure, one would expect to see a maximum area (top view) and a minimum area (thin line, side view) for a plate. However, TEM shows this pattern only for a few particles. Most particles are relatively uniform as they are tilted. This suggests their architecture is between a rod and a plate. Therefore, TEM tilt experiments show the aggregation of the primary $Cu(OH)_2$ rods occurs in three dimensions and not only as planar side-to-side attachments.

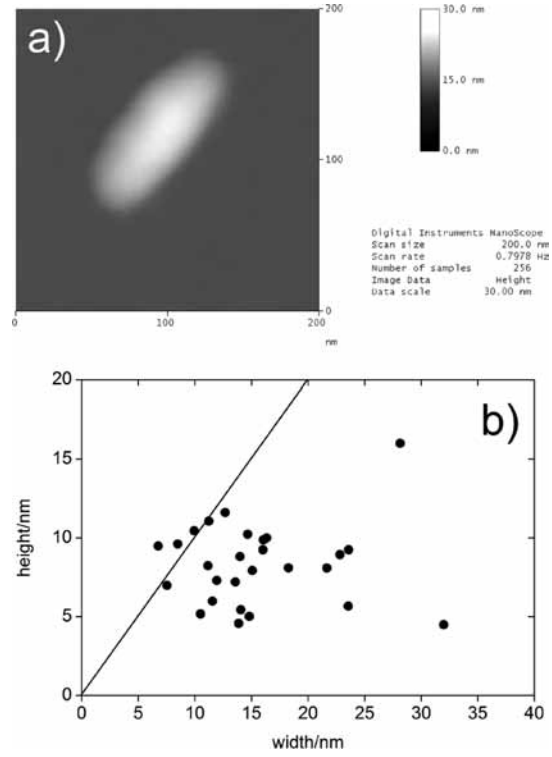

Figure 5. (a) AFM height image of a CuO particle on mica. (b) Plot of width versus height of some particles determined from AFM. The black line indicates a width/height ratio of one for perfect rods with equal width and height.

Figure 5 shows height and width data of the plates obtained from complementary atomic force microscopy (AFM) measurements. The average height is 8.3 ± 2.6 nm, and the average width is 15.6 ± 6.2 nm. For perfect rods, height and width should be identical and the width/height ratio (R) should be 1. However, Figure 5 clearly shows the CuO particles obtained here have a width/height ratio of about 1.9. Figure 5 also shows there are a few particles with $R \approx 1$. These particles are the smallest in the ensemble. Larger particles are wider but not thicker than the particles with $R \approx 1$. This suggests that the larger particles form by parallel attachment of smaller rods, which ultimately leads to the

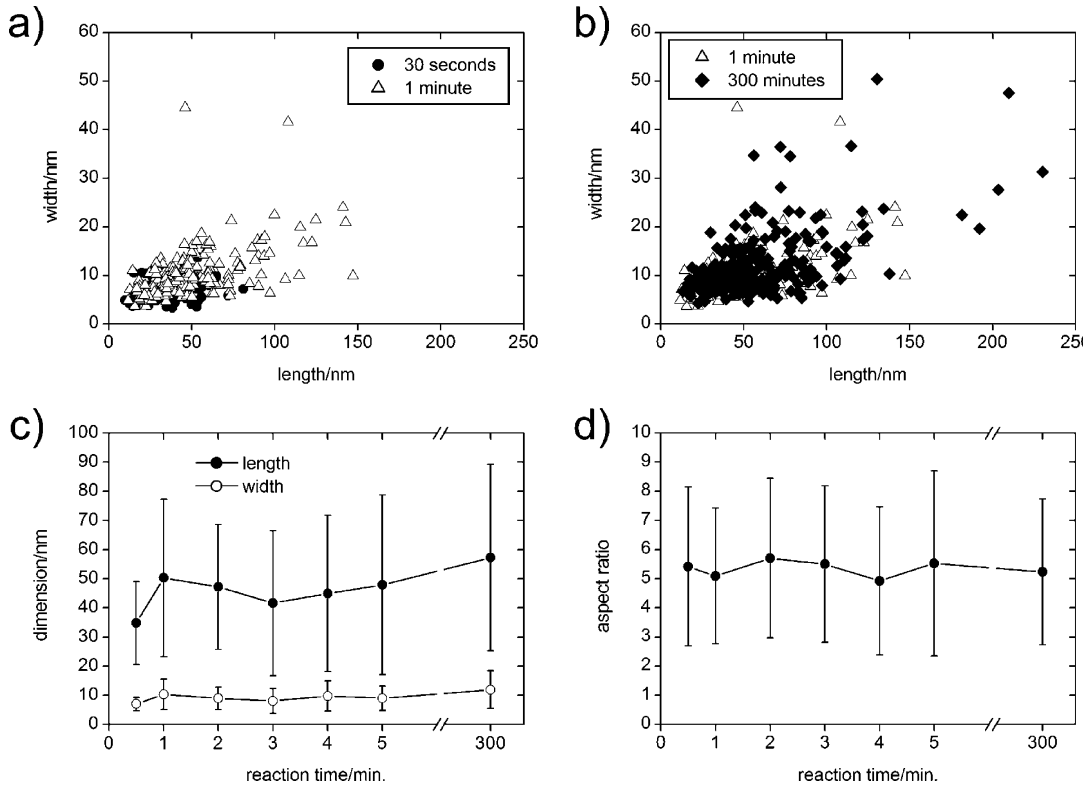

Figure 6. (a, b) Particle length versus width for samples grown at 100 °C for different reaction times showing the reaction time does not significantly affect the particle sizes. (c) Mean length and mean width of the same samples. (d) Mean aspect ratio of the same samples. For the 30 s reaction time, the dimensions refer to the individual nanorods; for all other reaction times, the dimensions refer to the aggregated plates.

somewhat larger particles observed after 5 min of reaction. These data are consistent with the TEM and HRTEM data, where we also found evidence for rod aggregation.

In summary, XRD and TEM suggest that $Cu(OH)_2$ rods precipitate initially. These rapidly aggregate and form well-defined CuO particles that are somewhat larger than the initial $Cu(OH)_2$ rods. HRTEM and SAED confirm the high crystallographic correlation, even across the boundaries of the individual primary rods. TEM tilt experiments and AFM show that the particles are only partly plates, and the average width/height ratio is about 1.9.

For a more detailed understanding of the particle growth, we have performed time-resolved experiments. Figure 6 shows the size evolution of some samples obtained under different conditions. Plots of length versus width of the same particle show that the particle size increases from 30 s to 1 min of reaction time. Thereafter, no further growth of the length or width is observed. Even with long reaction times of up to 300 min, the size does not change further. Figure 6 also shows that the aspect ratio is identical throughout the reaction. As a result, Figure 6 demonstrates that the particle formation process is terminated already after 1 to 2 min, even if the reaction is conducted at only 40 °C. This shows that the nucleation of $Cu(OH)_2$ is a highly efficient process followed by rapid particle growth.

From the particle sizes and the yields of the respective reactions, particle numbers can be estimated.[55] Figure 7 shows that after 30 s of reaction time, the yield has already reached the level of longer reaction times by about 80%. Figure 7 also shows that reactions conducted at 40 °C consistently have the lowest yields, although the yields are in the same range at all of the reaction temperatures, but slightly higher yields are obtained at higher reaction temperatures.

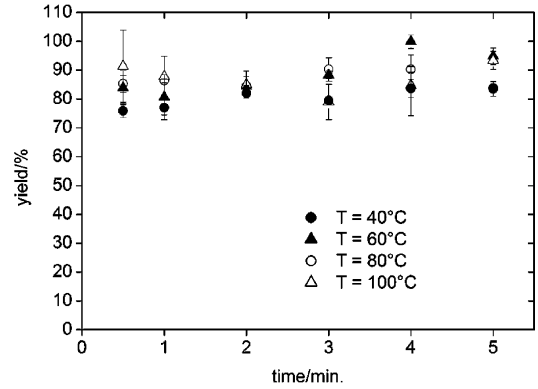

Figure 7. Yields of CuO formation versus reaction times for different reaction temperatures.

Table 1. Particle Numbers Calculated from Yield and Average Sizes

temperature (°C)	particle number after 30 s	particle number after 5 min
40	1.4×10^{15}	5.9×10^{14}
60	3.2×10^{14}	3.5×10^{14}
80	4.1×10^{14}	4.0×10^{14}
100	7.8×10^{14}	8.0×10^{14}

Table 1 shows the estimated particle numbers. Although they appear to be somewhat different, such data must be treated carefully. The estimation of particle numbers has some limitations mainly because of the particle-size distributions, which are difficult to determine exactly. As a result,

the data in Table 1 should be compared only by their order of magnitude, which is the same for all samples.

The only exception is the particle number obtained for the samples grown at 40 °C and 30 s. Here, the particle number is about 2.3 times larger than the particle number after 5 min. As this is the only case where we have observed smaller rods (Figure 2), and it is also the only case where $Cu(OH)_2$ has been observed directly (Figure 1), Table 1 further supports our aggregation-based growth model. Furthermore, Table 1 allows for the estimation of an average aggregation number, which is the average number of rods that form one plate. The average rod-per-plate number is 2.33, which is reasonably close to the numbers observed in the TEM images (Figure 2). We suspect that a small number of primary rods per final plate occurs because of the rapid dehydration of the $Cu(OH)_2$ rods to CuO, which would prevent further growth of the plate by the proposed condensation mechanism.

Summary and Conclusion

This work shows that after 30 s at temperatures above 40 °C, CuO formation in TBAH/water mixtures is already essentially complete. At 40 °C, the reaction is somewhat slower, but the final particle size, shape, and crystal phase are observed after 1 min. XRD and TEM show that the resulting plates form via a two-step process, where $Cu(OH)_2$ rods precipitate first. The rods aggregate and fuse into particles with a width/height ratio of about 1.9 and an average number of 2.33 rods per plate. HRTEM and electron diffraction show that the plates are single crystals and exhibit only some defects, which most likely originate from the assembly and fusion of the primary rods. The aggregation model is supported by the crystal structure of $Cu(OH)_2$ and CuO.[57,58] Both minerals have a layered structure, where Cu, O, and OH layers alternate. In both cases, the atomic layers are perpendicular to the long crystallographic axis. This favors the formation of the final particles because no defects or reorientation problems must be overcome during water elimination. In conclusion, this work demonstrates the growth of a seemingly simple material like CuO nanoplates can proceed via more complex pathways. Therefore, further study of mineralization in ILs and IL/water mixtures will be interesting.

Acknowledgment. We thank I. Zenke for help with the XRD measurements and A. Heilig for help with the AFM. We thank the Max-Planck-Institute of Colloids and Interfaces, (Colloid Chemistry Department), the University of Potsdam, the Potsdam Graduate School "Chemical Reaction in Green Solvents" (A.U.), and the Fonds der Chemischen Industrie for financial support.

IC801335K